

FABRICATION AND TESTING OF A HIGH-TEMPERATURE PRINTED CIRCUIT HEAT EXCHANGER

Minghui Chen, Xiaodong Sun^{*}, Richard N. Christensen

The Ohio State University
201 W 19th Ave, Columbus, OH 43210
chen.3370@osu.edu, sun.200@osu.edu

Isaac Skavdahl, Vivek Utgikar

University of Idaho
Idaho Falls, ID 83844

Piyush Sabharwall

Idaho National Laboratory
Idaho Falls, ID 83404

ABSTRACT

One of the very-high-temperature gas-cooled reactors' (VHTRs) missions is to produce electricity and provide process heat for applications with high efficiency and high safety. The electricity generation or process heat applications of VHTRs greatly rely on an effective intermediate heat exchanger (IHX) that transfers heat from the primary fluid (i.e., helium) to the secondary fluid, which can be either helium, molten salt, water/steam, or supercritical carbon dioxide. The IHX performance is directly related to the efficiency and safety of the overall nuclear system. A printed circuit heat exchanger (PCHE) is one of the leading IHX candidates due to its high compactness and effectiveness, as well as its robustness.

In the current study, a reduced-scale PCHE is fabricated using Alloy 617 plates for the heat exchanger core and Alloy 800H pipes for the headers. In this paper, PCHE fabrication processes, i.e., photochemical etching, diffusion bonding and brazing, are described. This PCHE has eight hot and eight cold plates with 11 semicircular wavy (zigzag) channels in each plate with the following channel dimensions: 1.2 mm hydraulic diameter, 24.6 mm pitch in the flow (stream-wise) direction, 2.5 mm pitch in the span-wise direction, and 15° wavy pitch angle. The thermal-hydraulic performance of the PCHE is investigated experimentally in the high-temperature helium test facility (HTHF) at The Ohio State University. The PCHE inlet temperatures and pressures are varied up to 350 °C/2 MPa for the cold side and 700 °C/2 MPa for the hot side, respectively, while the maximum mass flow rates of helium on both sides of the PCHE reach 30 kg/h. The corresponding maximum channel Reynolds numbers for both the hot and cold sides are about 3,000, covering the laminar flow and laminar-to-turbulent transitional flow regimes. Comparisons between the obtained experimental data and available empirical correlations in the literature show that both the hot-side and cold-side friction characteristics of the PCHE with the wavy channels follow the trend established in the empirical model well, while relatively large deviations are presented in the low Reynolds number region. Heat transfer characteristics obtained from the models that are available in the literature present some discrepancies from the current experimental data. Large deviations in heat transfer appear in the low Reynolds number region as well. A new heat transfer correlation based on the experimental data has been subsequently proposed for the current wavy-channel PCHE.

KEYWORDS

PCHE, thermal-hydraulic performance, compact heat exchangers, VHTR, diffusion bonding

1. INTRODUCTION

Advanced nuclear reactors such as the very-high-temperature gas-cooled reactors (VHTRs) from the Generation IV Program are endowed with electricity production and industrial process heat capabilities. The VHTRs are designed with the capability of delivering high-pressure, high-temperature helium to a power conversion unit (PCU) for electricity production and an industrial plant for process heat application. The helium temperature at the reactor core outlet is designed to be 750~800°C during the first development phase and is expected to be increased in the later development. With such high temperatures, VHTRs offer a wide range of applications. The electric power production may use Rankine cycle with a high-pressure steam generator, or a direct Brayton cycle gas turbine using the primary helium coolant as the working fluid, or an indirect-cycle gas turbine using a secondary fluid, such as helium or supercritical carbon dioxide [1]. The process heat applications may include hydrogen production, petroleum refining, bio-fuels production, and production of chemical feed stocks for use in the fertilizer and chemical industries [2]. The electricity production and process heat applications of VHTRs are critically dependent upon an effective intermediate heat exchanger (IHX), which is a key component in transferring the thermal energy from the primary coolant to the secondary coolant.

The IHX serves to isolate the reactor system from electricity generation and process heat application plants, and therefore must be robust enough to maintain the system integrity during normal and off-normal conditions. Since helium typically has a low heat transfer capability due to its low volumetric thermal capacity and low thermal conductivity, a compact heat exchanger with a high surface area to volume ratio (generally, higher than 700 m²/m³ [3]) is preferable to be employed as an IHX in the VHTR. The printed circuit heat exchanger (PCHE) stands out from several heat exchanger candidates due to its high effectiveness, high robustness, high compactness, and its ability to withstand high pressures [4]. PCHEs are plate-type compact heat exchangers in which flow channels (typically, channels with a small hydraulic diameter) are etched into flat metal plates using a photochemical machining process. There are several types of PCHE with respect to the channel geometry, such as straight channel, wavy (zigzag) channel, S-shape finned channel, and airfoil finned channel. The etched metal plates are then grinded and lapped to remove scratches on the plates and make the etched plates flat and parallel. Finally, the plates are stacked together with a prescribed arrangement configuration and diffusion bonded to create a high-integrity solid block before flow distribution headers are attached to the heat exchanger block.

Over the last decade, extensive studies related to PCHEs have been conducted in the U.S., Japan, and South Korea. Dostal [5] adopted a PCHE in a supercritical CO₂ Brayton power cycle to perform a system design evaluation in the next generation nuclear plant (NGNP). Gezelius [6] investigated the intrinsic characteristics of a straight-channel PCHE that coupled a helium-cooled fast reactor to a supercritical CO₂ Brayton power cycle. Chen et al. [7] performed a transient analysis of a fluoride salt-cooled high-temperature reactor (FHR) coupled to a helium Brayton power cycle using a PCHE-type secondary heat exchanger (SHX). Nikitin et al. [8] investigated heat transfer and pressure drop characteristics of a 3-kW PCHE with a compactness of 1050 m²/m³ in a supercritical CO₂ loop. Ngo et al. [9] investigated experimentally the thermal-hydraulic characteristics of PCHEs with wavy (zigzag) channels and S-shape finned channels. Both PCHEs had higher heat transfer performance than the conventional shell-and-tube heat exchangers. The PCHE with wavy channels gave a 24-34% higher Nusselt number than the PCHE with S-shape finned channels. However, the pressure drop with the wavy channels was 4-5 times larger than that in the S-shape finned channels for the same Reynolds numbers. Kim et al. [10] designed a PCHE for a 600-MW_{th} VHTR and the PCHE was optimized based on analyses of the capital cost and operational cost. Several factors, such as geometrical parameters, reactor thermal duty, lifetime, and working fluids, were analyzed and included in the optimum sizing model. Kim [11] conducted comprehensive numerical and experimental studies on a wavy-channel PCHE based on helium-helium, helium-water, and mixture (helium and CO₂)-water working fluid combinations. Correlations for calculating the Fanning friction factor and Nusselt number were proposed for wavy-channel PCHEs based on different channel angles,

itches, and hydraulic diameters. Yoon et al. [12] concluded that the wavy-channel PCHEs had the best performance over other channel geometries and configurations due to the wavy channel's high heat transfer capability, but low pressure drop characteristics in the laminar flow operating region.

Mylavarapu [2] designed and constructed a high-temperature helium test facility (HTHF) that can facilitate PCHE testing using helium as the working fluid at temperatures and pressures up to 800°C and 3 MPa with mass flow rates ranging from 15 to 49 kg/h. Meanwhile, two similar straight-channel PCHEs were fabricated using Alloy 617 plates with Alloy 800H headers and were installed in the HTHF in a counter flow configuration for testing thermal-hydraulic performance. The author proposed correlations for determining the hydrodynamic entrance length in a semicircular duct and the friction factor in the hydrodynamic entrance region for laminar flow in the semicircular duct based on the apparent Fanning friction factor.

Most of prior studies focused on the thermal-hydraulic performance of commercial PCHEs under low-temperature conditions. Limited research has been conducted on the performance of wavy-channel PCHEs under high-temperature helium conditions. Most of the research used acquired PCHEs from a commercial vendor with agreement of not to perform a destructive testing on the PCHEs. In the process of experimental data reduction, large uncertainties may be encountered in correlations due to the detailed geometrical parameters not being made available to the customers. The aim of the current research is therefore to address these issues. In this paper, a detailed fabrication procedure of a counter flow PCHE with wavy channels that can be used in high-temperature, high-pressure conditions is presented. Thermal-hydraulic performance testing of the wavy-channel PCHE is conducted in the HTHF at temperatures and pressures up to 700 °C and 2 MPa, respectively. The experimental data are compared with available correlations for the wavy-channel PCHEs.

2. PCHE THERMAL-HYDRAULIC DESIGN

Heat transfer and pressure drop play a significant role in the PCHE sizing or design process. Although the models/correlations for designing commercial PCHEs are proprietary to vendors and hence are not available to the public, extensive studies have been conducted to develop thermal-hydraulic models for designing a variety of PCHEs over the last decade. Kim [11] conducted both numerical and experimental studies for wavy-channel PCHEs under high-pressure helium to helium conditions and developed heat transfer and pressure drop models for wavy-PCHEs with different channel pitch angles and channel diameters. Figure 1 shows individual channels are etched in a wavy configuration. The geometry of the wavy channel is determined by the channel pitch angle ϕ and pitch length in the flow direction as indicated in the figure.

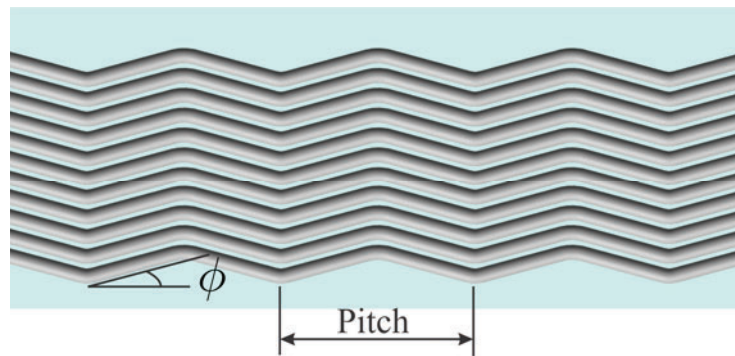


Figure 1. Wavy-channel Geometry.

Kim [11] developed correlations for the Fanning friction factor and Nusselt number for the wavy flow channels that are Reynolds number dependent as

$$f Re = 15.78 + 0.06677 Re^{0.71258} \quad (1)$$

$$Nu = 4.089 + 0.0083 Re^{0.86054} \quad (2)$$

where $300 < Re < 2,500$, the calculations of Reynolds number are based on the hydraulic diameter of semicircular channels. Following the thermal design method described in Bartel et al. [13], the size of a wavy-channel PCHE for helium to helium heat transfer is determined and the results are listed in Table I. Note that mass flow rates on both the cold and hot sides of the PCHE are identical.

Table I. Design results of the wavy-channel PCHE

Variables	Results	Variables	Results
Thermal power, kW	13	Total number of plate	16
Hot-side inlet temperature, °C	800	Plate thickness, mm	1.6
Cold-side inlet temperature, °C	350	Flow length, m	0.203
Hot-side outlet temperature, °C	462	Hot-side Nusselt number	9.2
Cold-side outlet temperature, °C	688	Cold-side Nusselt number	9.6
LMTD, °C	112	Hot-side heat transfer coefficient, W/m ² -K	2,473
Hot-side inlet pressure, MPa	2	Cold-side heat transfer coefficient, W/m ² -K	2,353
Cold-side inlet pressure, MPa	2	Overall heat transfer coefficient, W/m ² -K	1,206
Mass flow rate, kg/h	26.45	Hot-side pressure drop, kPa	2.3
Hot-side Reynolds number	1,753	Cold-side pressure drop, kPa	2.0
Cold-side Reynolds number	1,915	Plate material	Alloy 617

3. FABRICATION TECHNIQUES AND DESIGN ASPECTS

Following the design of the wavy-channel PCHE, the heat exchanger has been fabricated using 1/16-inch (1.6-mm) thick Alloy 617 plates. A total of eight hot plates and eight cold plates are diffusion bonded together to form a metal block with 11 wavy channels in each of the plates. Figure 2 shows the geometrical information for both the hot-side and cold-side plates of the PCHE. The cross section of the fluid passages is approximately semicircular with a diameter of 2 mm and a pitch of 2.5 mm in the span-wise direction. The shape of the flow passage is wavy, and the angle between the flow direction and the edge of the block is 15 degree, as shown in Figure 2. The PCHE is designed in such way that each side can withstand the maximum design pressure of 3 MPa in the HTHF.

The flow passages in each plate of the PCHE are made by applying a photochemical etching technique, which uses strong chemical etchants to remove the selected area on the surface of the plates. Four 20.7-mm diameter through holes and four 6.35-mm diameter small through holes are also made on each of the 16 plates during the chemical etching process. Figure 3 shows an exploded view and a schematic of the entire PCHE. Two 12.7-mm thick plates, one on the top of the heat exchanger block and the other at the bottom, are also applied to provide an added strength to the PCHE block. Four out of eight holes are used to direct the flow into and out of the channels. At the topmost plate, the four larger holes are connected to four headers. The other four smaller holes are used for alignment during the diffusion bonding process. Four pins are inserted into the four smaller holes before diffusion bonding to prevent the plates from sliding when adding large load on to the PCHE block to facilitate the diffusion bonding process. The

dimensions of the PCHE block shown in Figure 3 are 13.35 inches (339.1 mm) in length by 4.96 inches (126 mm) in width by 2 inches (50.8 mm) in height. The thicknesses of both the topmost plate and bottommost plate are 0.5 inch (12.7 mm). The topmost plate provides a strong base for joining the four headers. The headers are made from 1 inch NPS Alloy 800H pipes since the piping size in the test facility is 1 inch NPS (corresponding to a pipe schedule of 160).

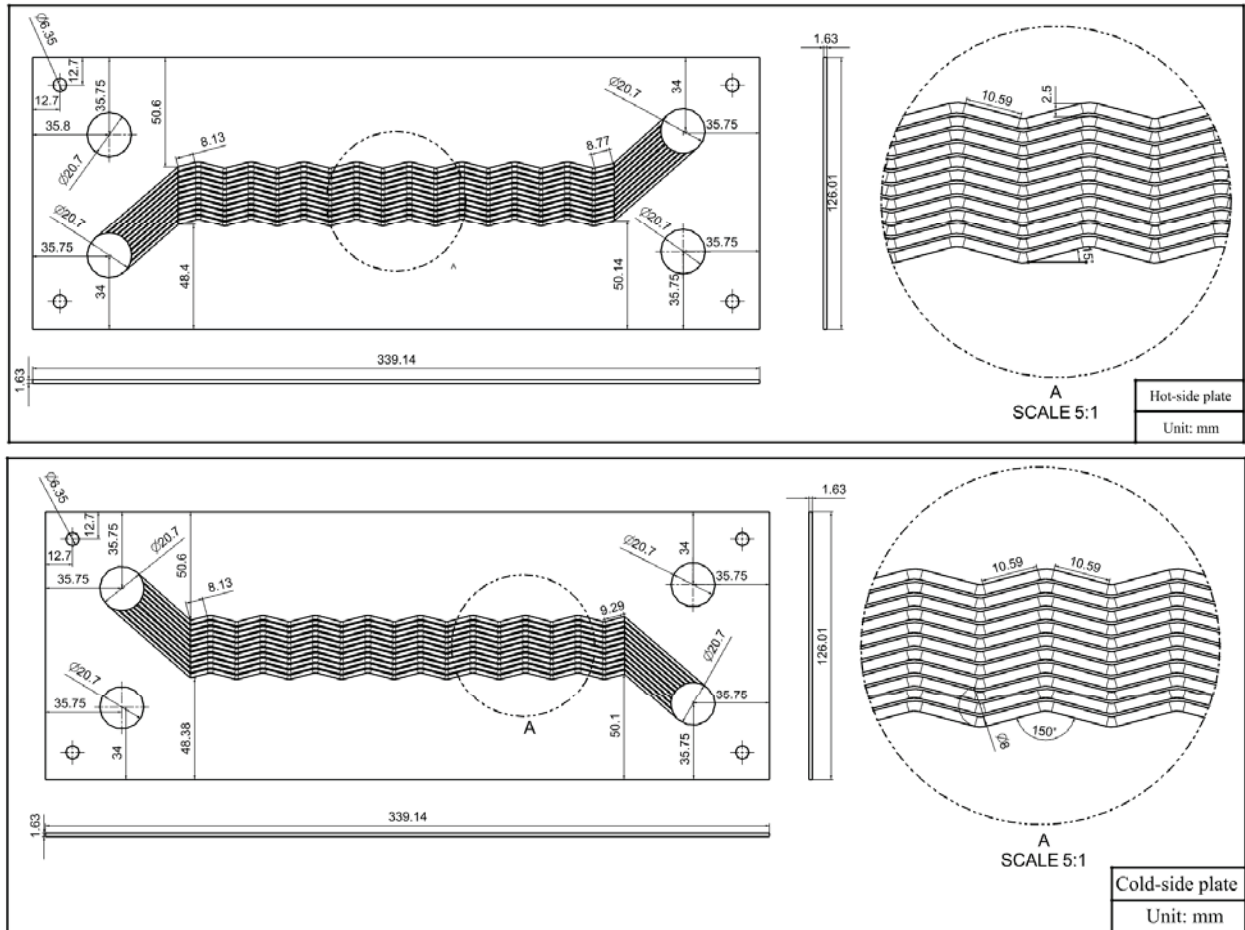


Figure 2. 2-D Drawings of the Wavy-channel PCHE Hot-side Plate and Cold-side Plate.

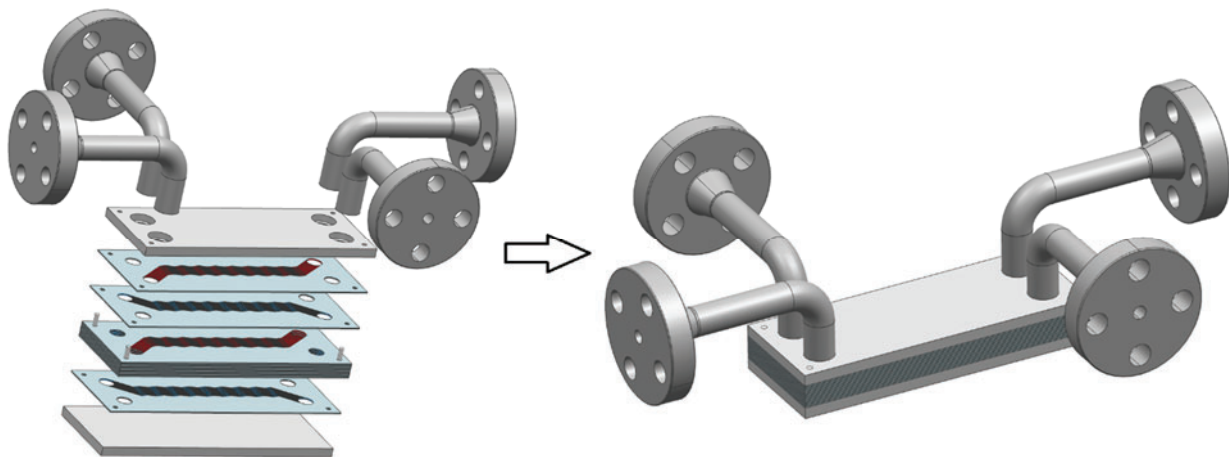


Figure 3. An Exploded View and a Schematic of the entire PCHE.

Once the photochemical etching process is completed, all the hot-side and cold-side plates are stacked alternately together, and put into a furnace to be diffusion bonded. Diffusion bonding is a solid-state joining technique, creating a monolithic joint at the atomic level [14]. Before diffusion bonding, it should be considered prudently as to how to connect the four headers to the PCHE block. Two approaches are discussed here: one is to perform the diffusion bonding after welding the four headers on to the topmost plate, while the other is to bond the plates together while simultaneously brazing the tubes on to the topmost plate. Figure 4 shows the schematic of these two approaches to join the four headers onto the PCHE bonded block.

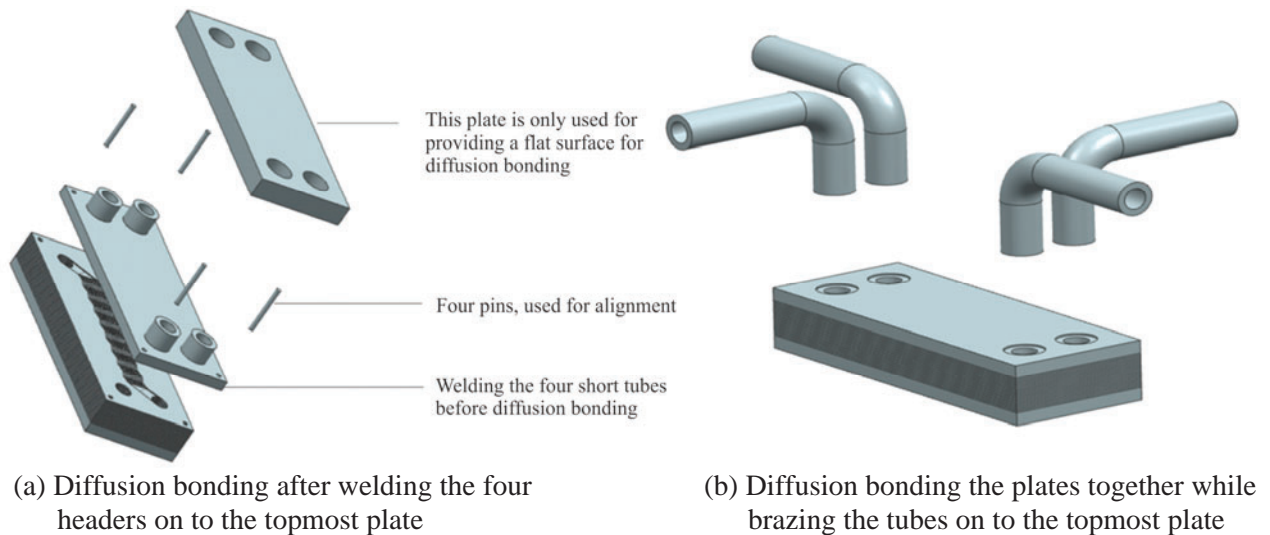


Figure 4. Schematic of Two Approaches to Join the Four Headers onto the PCHE Block.

The most common way to connect four headers to the PCHE block is to weld four headers on to the topmost plate after all the plates are diffusion bonded. These headers could be welded on to the diffusion bonded blocks by the Gas-Tungsten Arc Welding (GTAW) technique or other welding techniques with Alloy 617 as the filler material. In this process, damage may be caused to the PCHE bonded block due to the large thermal stress from the welding process. To reduce any potential thermal gradients and localized thermal stresses, four short tubes (see Figure 4) are welded on the topmost plate before diffusion bonding and other connecting tubes are welded on these four short tubes. The four short tubes provide a distance between the welding locations and the PCHE block, hence reducing the thermal gradients in the bonded block. Welding tubes onto the topmost plate before diffusion bonding can relieve the local stress and it does not negatively affect the welding quality. However, it is challenging and expensive to weld the tubes from the bonding surface side because the bottom surface of the topmost plate could deflect due to the large thermal gradient from the welding. Therefore, grinding the bottom surface back to its original flat state is required before bonding. In addition, a supporting plate has to accommodate the weld fillet radius and thus pushes the effective loading area away from the tubes. It might not be an issue, but taken to the extreme, it may cause channel crosstalk due to the unloaded area.

Brazing of four headers onto the PCHE bonded block was applied in the current study since it is an isothermal process and subsequently would not induce large stress on the diffusion bonds. Diffusion bonding the plates together while simultaneously brazing the tubes on to the topmost plate protects the integrity of the diffusion bonded block and brazed joints. However, the aluminum and titanium contents of Alloy 617 could cause incomplete wetting. The brazing parts should be plated with nickel before the brazing process to prevent incomplete wetting. In the present study, the second method, i.e., brazing four header on the PCHE bonded block, is adopted.

The fabrication of the reduced-scale PCHE was completed. Figure 5 shows a picture of the diffusion bonded stack and channel inlets on the plates. Through one of the headers, it can be seen that the inlet channels were lined and the inlet recession surface is smoothed.

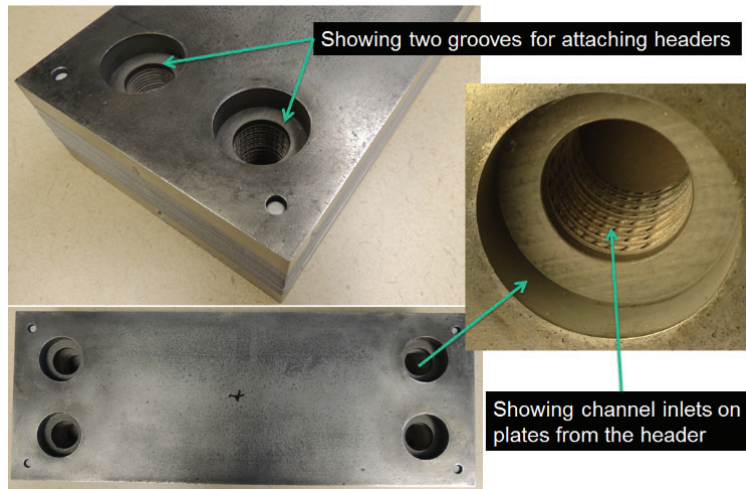


Figure 5. Photographs of the Diffusion Bonded Stack and Channel Inlets on Plates.

The leakage tests for the entire heat exchanger were conducted per ASTM helium leak test standard E493 by using a helium leak detector [15]. The diffusion bonded stack passed the leak test initially, but there was a leak at a brazed joint (at a leakage at about 6×10^{-9} l/sec) detected. Re-brazing was performed and the leak was fixed.

In summary, a wavy-channel PCHE is designed for a helium-helium working fluid combination and possesses a 13-kW nominal thermal load. The design pressure and temperature are 3 MPa and 800 °C, respectively. The PCHE block is made of Alloy 617 material and four headers are made from Alloy 800H pipes. The PCHE core dimension is 13.35'' \times 4.96'' \times 2'' (339.1 \times 126 \times 50.8 mm³) with eight plates on each of the hot and cold sides, consisting of 11 chemically-etched wavy channels on each plate. The actual assembly with four headers is shown in Figure 6.



Figure 6. PCHE with Four Headers Assembled.

4. PCHE PERFORMANCE TESTING

4.1. High-temperature Helium Test Facility

Experiments were performed to examine the thermal-hydraulic performance of the reduced-scale wavy-channel PCHE under steady-state conditions. The experimental study capitalized on the HTHF at The Ohio State University. Figure 7 shows the layout of the high-temperature helium test facility. The HTHF was constructed to facilitate thermal-hydraulic performance testing of heat exchangers at temperatures and pressures up to 800°C and 3 MPa, respectively [2]. The HTHF consists of pre-heater and main-heater to heat helium to high temperatures, a gas booster to boost the helium pressure to overcome the pressure drop, a cooler to cool helium down to low temperatures before returning to the gas booster, piping, valves, and various instruments. Pre-heater and main-heater are identical electric heaters with the same maximum heating capacity of 23 kW. Three heating elements, each having a maximum capacity of approximate 6.7 kW, are embedded on the inner surface of the ceramic fiber insulation and are virtually free-radiating. The maximum element temperature is 1,300 °C. The gas booster installed in the HTHF is a single-stage double-acting air-drive booster. The helium flow in the system has periodical fluctuations due to the reciprocating action of the booster. Therefore, an inline air-drive pressure regulator valve, in addition to a helium surge tank, was installed downstream of the booster to damp the flow oscillations in the system. In addition, all the measurement sensors have been calibrated against standards traceable to the National Institute of Standards and Technology (NIST). Two straight-channel PCHEs made of Alloy 617 and Alloy 800H were tested in this facility [2].

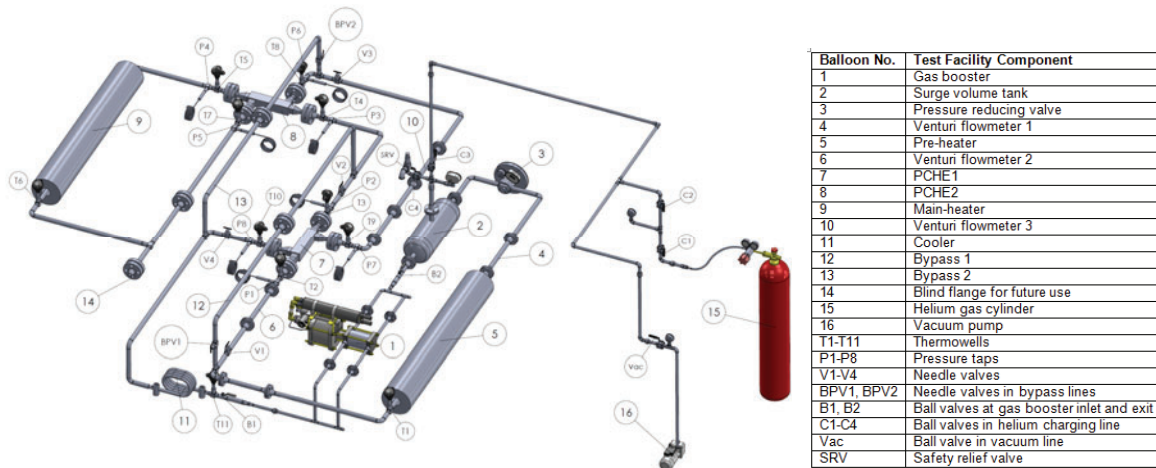


Figure 7. Layout of the High-temperature Helium Test Facility [16].

Figure 8 is a schematic showing the helium flow path for heat exchanger testing, when one of the two straight-channel PCHEs is replaced by the reduced-scale wavy-channel PCHE (i.e., the PCHE to be tested). When the test PCHE operates at the nominal steady-state condition, the inlet and outlet temperatures of these two PCHEs are also shown in Figure 8. The mass flow rate under the nominal steady-state operation is 26.5 kg/h. The thermal duties of the pre-heater and main-heater are 6.5 and 4.3 kW, respectively.

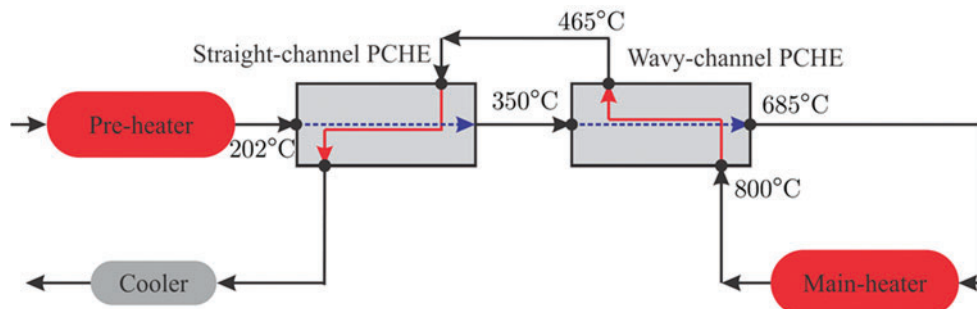


Figure 8. Schematic of the HTHF System Design with Heat Exchangers Included.

4.2 Experimental Data Reduction Method

4.2.1 Pressure drop contributions

The test PCHE was installed in the HTHF for the determination of its pressure drop and heat transfer characteristics. The first step is to determine the flow friction characteristics, i.e., the Fanning friction factor. The approach described by Chen [17] was adopted for this determination. Figure 9 displays the pressure drop measurement locations on one side of the PCHE. Two differential pressure transducers were installed on each side of the test PCHE to measure the pressure drops across the PCHE. The pressure drop associated with the heat exchanger is comprised of two major contributions: (1) pressure drop across the heat exchanger core and (2) pressure drop through fluid distribution devices such as inlet/outlet flow distribution headers [3].

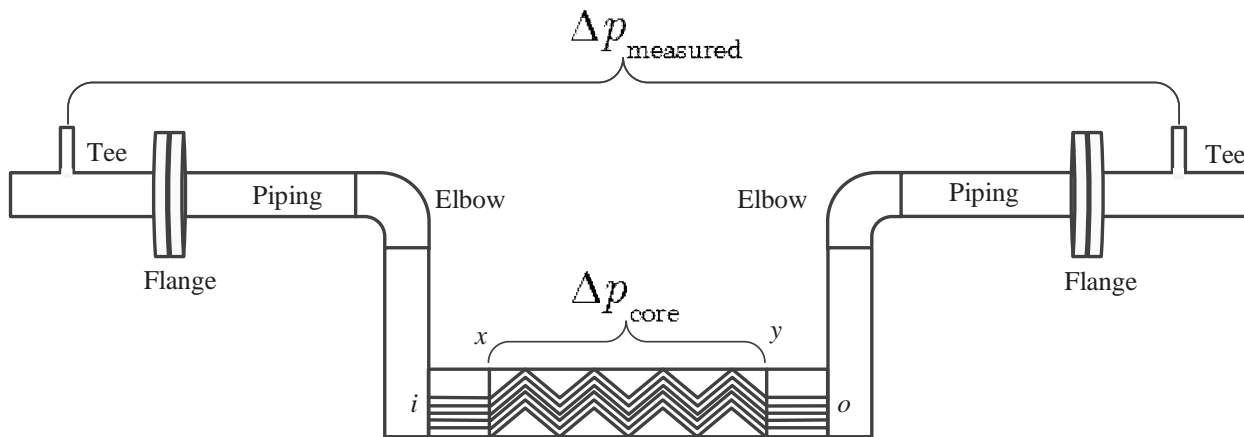


Figure 9. PCHE Set-up and Illustration of Pressure Drop Contributions.

It can be seen from Figure 9 that the total pressure drop measured on each side includes several contributors: pressure loss associated with the heat exchanger core; pressure loss associated with inlet/outlet flow entrance region; additional pressure loss at the straight-channel regions (i.e., regions between surfaces i and x , and y and o as shown in Figure 9) at the inlet/outlet of the exchanger; and pressure loss associated with the piping, fittings (tees and elbows), and flanges between the differential pressure taps. Therefore, factors that cause pressure drop in the current PCHE are: (1) flow frictional losses in the exchanger core; (2) flow momentum rate change; (3) pressure drop associated with sudden contraction at the channel inlets; (4) pressure change associated with sudden expansion at the channel exits; (5) straight-channel inlet and outlet regions; and (6) pressure drop in piping, fittings and flanges.

To determine the friction characteristics of the PCHE core, it is necessary to exclude the pressure drop contributions from the experimentally measured pressure drop values that are not associated with the heat exchanger core friction. Other pressure drops not related to the heat exchanger core pressure drop are subtracted with the help of available empirical correlations in the literature. The experimental Fanning friction factor is then estimated from the core pressure drop for the wavy channels of the PCHE. For the core frictional characteristics, hot-side and cold-side pressures are separately obtained under isothermal and elevated-temperature test conditions. The assumptions made for pressure drop analysis are as follows: (1) the incoming flow is steady; (2) the fluid is uniformly distributed into each of the channel from the headers; (3) the channel geometry is identical for all channels on each of the cold and hot sides; (4) gravity effect is neglected since the heat exchanger is horizontally oriented; and (5) the cross sections of the flow channel passages are exactly semicircular. The total measure pressure drop is the sum of all the pressure drop contributions and is expressed as

$$\Delta p_{measure} = \left(\frac{G^2}{2\rho_i} \right) \left[(1 - \sigma^2 + K_c) - (1 - \sigma^2 - K_e) \left(\frac{\rho_i}{\rho_o} \right) \right] + \left(\frac{G^2}{2\rho_i} \right) \left[2 \left(\frac{\rho_i}{\rho_o} - 1 \right) + 4f \left(\frac{l}{d_h} \right) \rho_i \left(\frac{1}{\rho} \right)_m \right] + \left(\Delta p_{straight-channel regions} + \Delta p_{fittings} + \Delta p_{piping} + \Delta p_{flanges} \right). \quad (3)$$

The variables are referred to the Nomenclature. Fanning friction factor, f , the only unknown in Eq. (3), can be determined from the experimental data.

4.2.2 Heat transfer coefficient

In the present study, no local internal fluid and wall temperature measurements are available. Therefore, local heat transfer coefficient and mean convective heat transfer on either side of the heat exchanger cannot be obtained directly. From the PCHE fabrication aspects, the hot-side heat transfer area, $A_{s,h}$, and the cold-side heat transfer area, $A_{s,c}$, are the same, i.e., $A_{s,h} = A_{s,c} = A_s$. The overall thermal resistance can be expressed as

$$\frac{1}{UA_s} = \frac{1}{h_h A_{s,h}} + \frac{1}{h_c A_{s,c}} + R_w. \quad (4)$$

From References [8, 11], the heat transfer model is an only function of the Reynolds number. The heat transfer coefficient for either side can be calculated from the Nusselt number that can be expressed as

$$Nu = c Re^a, \quad (5)$$

where a and c are constants. Therefore, the local heat transfer coefficient h is given by

$$h = \frac{Nu\lambda}{d_h} = \frac{c Re^a \lambda}{d_h}, \quad (6)$$

where λ is the thermal conductivity of the fluid and d_h is the channel hydraulic diameter. Substituting Eqs. (5) and (6) into Eq. (4), Eq. (4) can be written as

$$\frac{1}{Ud_h} = \frac{1}{c Re_h^a \lambda_h} + \frac{1}{c Re_c^a \lambda_c} + \frac{R_w A_s}{d_h}, \quad (7)$$

where U , Re , R_w , and λ can be obtained from the experiments; A and d_h are geometrical parameters. Two unknown constants a and c can be solved by using nonlinear regression method to minimize the residual S as:

$$S = \sum_{j=1}^N \left[\frac{1}{U_j d_h} - \frac{R_w A_s}{d_h} - \frac{1}{c Re_{h,j}^a \lambda_{h,j}} - \frac{1}{c Re_{c,j}^a \lambda_{c,j}} \right]^2, \quad (8)$$

where N is the total number of the available experimental data points. Once a and c are determined, the Nusselt number correlation (i.e., Eq. (5)) is confirmed. The heat transfer coefficients for both sides can be calculated separately from the Nusselt numbers. In addition, the average wall temperature can be obtained via the heat transfer coefficients on both the hot and cold sides.

To determine the overall heat transfer coefficient of the reduced-scale wavy-channel PCHE, it is necessary to obtain the effective heat transfer area and consider the heat transfer contributions inside the heat exchanger. Figure 10 is a schematic of the effective heat transfer area and heat conduction between the two adjacent ports. The heat transferred from the hot side to the cold side consists of several contributions: (1) heat conduction from port #1 to port #2 and from port #3 to port #4; (2) heat transfer in the crossflow configurations in X and Y regions; (3) heat transfer in the countercurrent flow region Z; and (4) heat loss to the surroundings. Four thermocouples were installed at locations 1, 2, 3, and 4 (see Figure 10) in the HTHF to measure the inlet and outlet temperatures of the heat exchanger.

Three experimental data points are used to examine the heat conduction from port #1 to port #2 and from port #3 to port #4, i.e., contribution #1 mentioned above. The average ratio of the total heat conduction to the total heat transferred from the hot side to the cold side is about 0.4%, whereas the overall heat transfer coefficient is 1.1% higher than that without considering this heat conduction. Changes in the four terminal temperatures result in the LMTD decreasing by 1.1%. A smaller LMTD gives a larger overall heat transfer coefficient when the heat conduction (contribution #1) between the ports is neglected. Note that the heat transfer area summation of regions X, Y, and Z, showing in Figure 10, is the effective heat transfer area that is adopted in the current study.

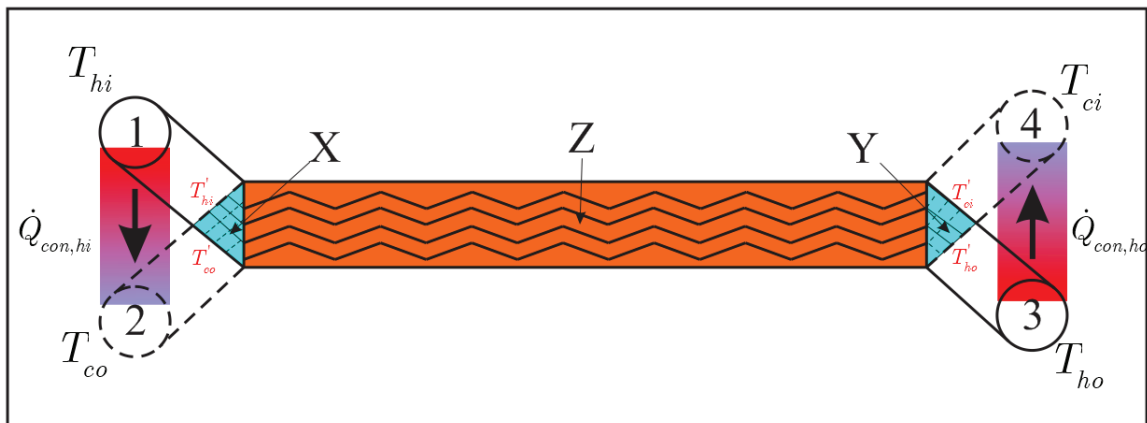


Figure 10. Schematic of the Effective Heat Transfer Area and Heat Conduction Path (1, 2, 3, and 4 Represent the Hot-side and Cold-side Ports or Plena).

4.2.3 Uncertainty analysis

An uncertainty analysis, considering error propagation, has been performed using the root-sum-square method. The uncertainty in the Fanning friction factor is based on the simplified form of the heat exchanger core friction pressure drop given by

$$f = \frac{\Delta p}{2} \frac{d_h}{l} \frac{\rho A_c^2}{\dot{m}^2}. \quad (9)$$

The uncertainty in Fanning friction factor can be expressed as

$$\frac{\delta f}{f} = \sqrt{\left(\frac{\delta \Delta p}{\Delta p}\right)^2 + \left(\frac{\delta d_h}{d_h}\right)^2 + \left(2 \frac{\delta \dot{m}}{\dot{m}}\right)^2 + \left(2 \frac{\delta A_c}{A_c}\right)^2 + \left(\frac{\delta l}{l}\right)^2 + \left(\frac{\delta \rho}{\rho}\right)^2}. \quad (10)$$

The heat transfer model is obtained by using the nonlinear regression method. The perturbation method is used to determine the uncertainties in the fitted heat transfer correlation [18], i.e., uncertainties in constants a and c in Eq. (5). The uncertainties in Re_h , Re_c , λ_h , λ_c , A_c , d_h and R_w in Eq. (8) can be determined from the experimental data. One of the seven variables is changed to its upper bound and the corresponding values of a_1 and c_1 are determined. These values are compared with the original least squares values to determine Δa_1 and Δc_1 . The same procedure is repeated for its low bound value in the same variable, Δa_2 and Δc_2 are then obtained. These steps are repeated for the remaining variables. There are fourteen regression runs required to compute all individual relative errors in constants a and c . Finally, the uncertainties in a and c are calculated separately by taking the root-mean-square method as:

$$\begin{cases} \delta a = \sqrt{\frac{1}{n} \sum_{i=1}^n (\Delta a_i^2)} \\ \delta c = \sqrt{\frac{1}{n} \sum_{i=1}^n (\Delta c_i^2)} \end{cases}, \quad (11)$$

where n is the number of the regression runs.

4.3 Preliminary Experimental Data Analysis

Preliminary performance testing of the wavy-channel PCHE has been carried out. The test loop was charged with helium to a desired pressure from the helium gas cylinder with a purity rating of 99.9999% after the test loop was vacuumed to the desired vacuum pressure of -14 psig by using a vacuum pump. The cooler was turned on during all the tests to avoid high-temperature helium going through the gas booster and damaging it. The helium flow in the test loop was driven by the gas booster. Before data processing, the mass flow rates were checked for all experimental runs and the oscillations of the mass flow rates recorded by two Venturi flow meters installed in the HTHF were less than 1% of their respective mean values.

4.3.1 Pressure drop characteristics

The experimentally obtained isothermal Fanning friction factors were compared with those obtained by Kim's friction factor correlations [11] that were used in the PCHE thermal design. Figures 11 and 12 show the plots of the experimental Fanning friction factor compared with the results obtained from Kim's correlations for both the hot and cold sides of the PCHE. As can be seen from the figures, the experimentally obtained Fanning friction factors follow the trend established in Kim's model well, while discrepancies between the experimental data and the correlations are presented mainly due to the channel differences. Kim used wavy channels with sharp turns at all of the bends, whereas a radius of curvature was induced at each bend in all channels of the test PCHE. The cross section is not exactly a semicircular shape in the test PCHE, while Kim's numerical model is for wavy channels with a perfect semicircular cross section. Compared to the experimental data, the largest differences with Kim's model are 19.8% and 32.1% for the hot side and cold side, respectively. The discrepancies between the experimental data and

numerical results are presented since the pressure drop in the laminar flow region is strongly dependent on the geometry and size of the flow channel.

The Fanning friction factors on the hot and cold sides are different, which is attributed to the flow channel geometry as well. The channels geometric parameters on the hot and cold sides are not exactly identical due to manufacturing imperfections and tolerance. For both the hot and cold sides, the uncertainties are 17.2% and 23.4% for the Fanning friction factors reduced from the data at the smallest Reynolds number and the largest Reynolds number, respectively.

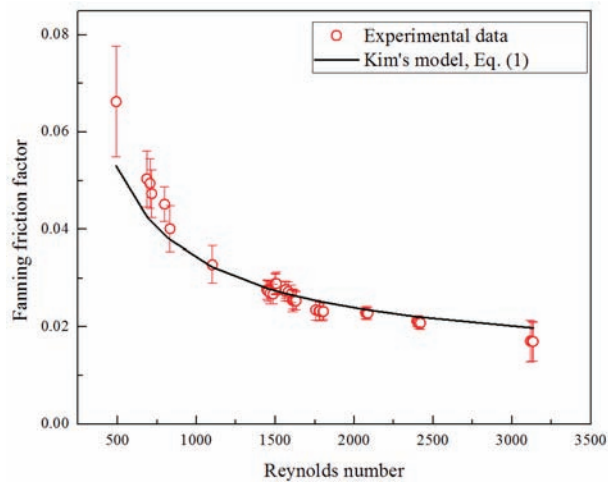


Figure 11. Fanning Friction Factor on the Hot Side.

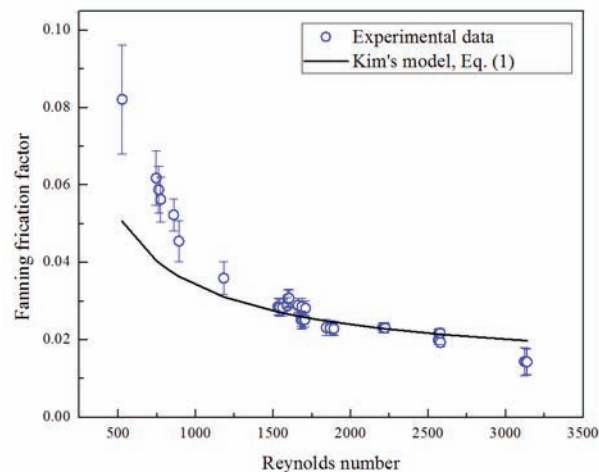


Figure 12. Fanning Friction Factor on the Cold Side.

4.3.2 Heat transfer characteristics

Equation (12) is the fitted heat transfer correlation with uncertainties in the constants identified, which is obtained by following the method described in Sections 4.2.2 and 4.2.3. The fitted experimental correlation, as shown in Figure 13, indicates that the Nusselt number increases gradually with the increasing Reynolds number. The increase of the Nusselt number with increasing the Reynolds number occurs due to the velocity increase, resulting in a more turbulent fluid flow. As the Reynolds number decreases, the turbulence in the flow tends to decrease and eventually diminish. As a result, the heat transfer coefficient decreases. The open-stared line as shown in Figure 13 presents the upper limit of the

fitted Nusselt number, which can be obtained by changing constants a and c to their upper bounds. When a and c are given to their lower bounds, the lower limit of the fitted Nusselt number is obtained, as shown in open-triangled line in Figure 13.

Figure 13 also shows the comparison between the Nusselt numbers from the experiments and from Kim's model (open-circled line). Results obtained from Kim's model show some discrepancies with the current correlation. Kim's model presents a slower Nusselt number increase rate with the increase of Reynolds number than the current correlation. Larger deviations can be seen in the low Reynolds number region where the current correlation gives smaller Nusselt number values than the model developed by Kim. As the Reynolds number increases, the differences between the two results decrease from 31.6% to 0.4%. Nusselt number is strongly dependent on the channel geometry and boundary conditions in laminar flow regime. As described in Section 4.3.1, the channel geometry used in the present study is different from that used in Kim's simulation. In addition, the boundary condition of Kim's modeling is constant wall heat flux with constant circumferential wall temperature. However, the actual testing boundary condition in our experiments is much more complicated and may not reflect the condition used in the Kim's model.

$$Nu = c Re^a$$

$$c = 0.028899 \pm 7.393333 \times 10^{-4}$$

$$a = 0.75508 \pm 1.95556 \times 10^{-3}$$
(12)

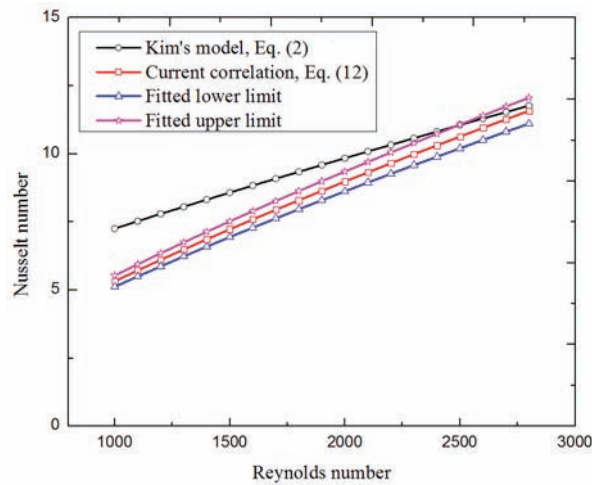


Figure 13. Nusselt Number for both the Cold and Hot Sides.

5. CONCLUSIONS

In this study, one reduced-scale PCHE was fabricated using Alloy 617 plates for the heat exchanger core and Alloy 800H pipes for the heat exchanger headers. The detailed fabrication techniques are presented. The thermal-hydraulic performance of the PCHE was investigated experimentally in the high-temperature helium test facility located at The Ohio State University. Comparisons between the obtained experimental data and available empirical correlations indicated that both the hot-side and cold-side friction characteristics of the PCHE follow the trend in the empirical model well. Heat transfer characteristics obtained from the experimental result show some discrepancies mainly due to the geometric differences. Larger deviations appear in the low Reynolds number region. Finally, the constants in the correlation for the convective heat transfer coefficient model for the wavy channels are proposed based on the experimental data.

NOMENCLATURE

a	constant in the heat transfer correlation, Eq. (5)
A_c	channel cross-section area
A_s	heat transfer area
c	constant in the heat transfer correlation, Eq. (5)
d_h	channel hydraulic diameter
f	Fanning friction factor
G	mass flux
h	heat transfer coefficient
K_c	contraction loss coefficient
K_e	exit loss coefficient
l	flow length
\dot{m}	mass flow rate
n	number of regression runs
N	number of experimental data points
Nu	Nusselt number
Δp	pressure drop
\dot{Q}	heat conduction rate in Figure 10
R_w	wall thermal resistance
Re	Reynolds number
S	residual
T	temperature
U	overall heat transfer coefficient
x, y	wavy channel inlet and outlet surfaces
X,Y,Z	effective heat transfer regions in the test PCHE

Greek symbols

ρ	helium density
δ	uncertainty
ϕ	wavy pitch angle
σ	ratio of heat exchanger core minimum free-free area to frontal area
λ	helium thermal conductivity

Subscripts

c	cold side
h	hot side
i	inlet
j	j^{th} experiment, index
m	mean value
o	outlet

ACKNOWLEDGEMENTS

This research is being performed using funding received from the U.S. Department of Energy Office of Nuclear Energy's Nuclear Energy University Programs. The assistance provided by Mr. Kevin Wegman of The Ohio State University is appreciated.

REFERENCES

1. P. Sabharwall, E.S. Kim, M. McKellar, and N. Anderson, "Process Heat Exchanger Options for the Advanced High Temperature Reactor," *INL/EXT-11-21584*, Idaho National Laboratory (2011).
2. S.K. Mylavarapu, "Design, Fabrication, Performance Testing, and Modeling of Diffusion Bonded Compact Heat Exchangers in a High-temperature Helium Test Facility," *Doctoral dissertation*, The Ohio State University (2011).
3. R.K. Shah and D.P. Sekulic, "Fundamentals of Heat Exchanger Design," John Wiley & Sons (2003).
4. Heatric, http://www.heatric.com/typical_characteristics.html, accessed on April 15th (2015).
5. V. Dostal, "A Super Critical Carbon Dioxide Cycle for Next Generation Nuclear Reactors," *Master thesis*, Massachusetts Institute of Technology (2004).
6. K. Gezelius, "Design of Compact Intermediate Heat Exchangers for Gas Cooled Fast Reactors," *Master thesis*, Massachusetts Institute of Technology (2004).
7. M. Chen, I.H. Kim, X. Sun, R.N. Christensen, V.P. Utgikar, and P. Sabharwall, "Transient Analysis of an FHR Coupled to a Helium Brayton Power Cycle," *Progress in Nuclear Energy*, **83**, pp. 283-293 (2015).
8. K. Nikitin, Y. Kato, and L. Ngo, "Printed Circuit Heat Exchanger Thermal-hydraulic Performance in Supercritical CO₂ Experimental Loop," *International Journal of Refrigeration*, **29**(5), pp. 807-814 (2006).
9. T.L. Ngo, Y. Kato, K. Nikitin, and T. Ishizuka, "Heat Transfer and Pressure Drop Correlations of Microchannel Heat Exchanger with S-shaped and Zigzag Fins for Carbon Dioxide Cycles," *Experimental Thermal and Fluid Science*, **32**, pp. 560-570 (2007).
10. E.S. Kim, C. Oh, and S. Sherman, "Simplified Optimum Sizing and Cost Analysis for Compact Heat Exchanger in VHTR," *Nuclear Engineering and Design*, **238**(10), pp. 2635-2647 (2008).
11. I.H. Kim, "Experimental and Numerical Investigations of Thermal-hydraulic Characteristics for the Design of a Printed Circuit Heat Exchanger (PCHE) in HTGRs," *Doctoral dissertation*, Korea Advanced Institute of Science and Technology (2012).
12. S.H. Yoon, H.C. No, and G.B. Kang, "Assessment of Straight, Zigzag, S-shape, and Airfoil PCHEs for Intermediate Heat Exchangers of HTGRs and SFRs," *Nuclear Engineering and Design*, **270**, pp. 334-343 (2014).
13. N. Bartel, M. Chen, V.P. Utgikar, X. Sun, I.H. Kim, R.N. Christensen, and P. Sabharwall, "Comparative Analysis of Compact Heat Exchangers for Application as the Intermediate Heat Exchanger for Advanced Nuclear Reactors," *Annals of Nuclear Engineering*, **81**, pp. 143-149 (2015).
14. B. Derby and E.R. Wallach, "Theoretical Model for Diffusion Bonding," *Metal Science*, **16**(1), pp. 49-56 (1982).
15. "Standard Test Methods for Leaks Using the Mass Spectrometer Leak Detector in the Inside-out Testing Mode," *ASTM E493-06*, ASTM International (2006).
16. S.K. Mylavarapu, X. Sun, R.E. Glosup, R.N. Christensen, and M.W. Patterson, "Thermal-hydraulic Performance Testing of Printed Circuit Heat Exchangers in a High-temperature Helium Test Facility," *Applied Thermal Engineering*, **65**, pp. 605-614 (2014).
17. M. Chen, "Design, Fabrication, Testing, and Modeling of a High-temperature Printed Circuit Heat Exchanger," *Master thesis*, The Ohio State University (2015).
18. H.F. Khartabil and R.N. Christensen, "An Improved Scheme for Determining Heat Transfer Correlations from Heat Exchanger Regression Models with Three Unknowns," *Experimental Thermal and Fluid Science*, **6**, pp. 808-819 (1992).